Use of novel high-resolution 3D marine seismic technology to evaluate Quaternary fluvial valley development and geologic controls on shallow gas distribution, inner shelf, Gulf of Mexico

Timothy A. Meckel[1] and Francis J. Mulcahy[2]

Abstract

The first deployment of the P-Cable™ high-resolution 3D (HR3D) seismic acquisition system in the Gulf of Mexico has provided unprecedented resolution of depositional, architectural, and structural features related to relative sea-level change recorded in the Quaternary stratigraphy. These details are typically beyond conventional 3D seismic resolution and/or excluded from commercial surveys, which are generally optimized for deeper targets. Such HR3D data are valuable for detailed studies of reservoir analogs, sediment delivery systems, fluid-migration systems, and geotechnical hazard assessment (i.e., drilling and infrastructure). The HR3D survey (31.5 km^2) collected on the inner shelf (<15 m water depth) offshore San Luis Pass, Texas, imaged the upper 500 m of stratigraphy using peak frequency of 150 Hz and 6.25 m^2 bin size. These data provided an exceptionally well-imaged example of shallow subsurface depositional system and stratigraphic architecture development during a lowstand period. The system evolved from a meandering channel with isolated point-bar deposits to a transgressive estuary characterized by dendritic erosional features that were eventually flooded. In addition, HR3D data have identified a previously unidentified seismically discontinuous zone interpreted to be a gas chimney system emanating from a tested (drilled) nonproductive, three-way structure in the lower Miocene (1.5 km depth). Within the shallowest intervals (<100 m) and at the top of the chimney zone, seismic attribute analysis revealed several high-amplitude anomalies up to 0.5 km^2. The anomalies were interpreted as reaccumulated thermogenic gas, and their distribution conforms to the stratigraphy and structure of the Quaternary interval, in that they occupy local fault-bounded footwall highs within remnant coarser-grained interfluvial zones, which are overlain by finer grained, transgressive deposits.

Introduction

The evolution of seismic technology has often focused on higher resolution and deeper observation. A more recent trend focuses on improved 3D imagery of the relatively shallow subsurface interval, called high-resolution 3D (HR3D) or ultrahigh resolution 3D (UHR3D). With penetration of 10 s to perhaps 1000 m, these data bridge a critical imaging gap between ultrashallow systems (e.g., 3D Chirp; Gutowski et al., 2008) and conventional 3D systems. The HR3D systems are defined depending mostly on the source frequency content recorded, bin size, and receiver sampling rate, all of which affect vertical and horizontal resolution. The relatively high frequency content reduces the depth of investigation to perhaps 2 s two-way traveltime (TWT), depending on source characteristics.

Development of shallow HR3D technology has been primarily driven by an evolving need to understand the shallow interval for geotechnical purposes (Marsset et al., 1998; Brookshire et al., 2015). A prominent early application related to mapping of offshore faults for evaluating seismic hazard near the Diablo Canyon Nuclear Power Plant in California (Ebuna et al., 2013). However, these types of systems are also being deployed for a variety of other applications, especially the investigation of natural geologic fluid flow systems and gas hydrates (Petersen et al., 2010). In some basins, such as the northern North Sea and the Barents Sea, economic reservoirs have recently been discovered at surprisingly shallow depths (e.g., the North Sea Peon Field; 15–30 billion standard cubic meters gas at 640 m subseafloor), and they are actively explored using HR3D systems. Shallow stratigraphic mapping can also identify sediment delivery systems on continental shelves and connect them to deep water settings (Pirmez et al., 2012). The use of UHR3D volumes of recent

[1]The University of Texas at Austin, Bureau of Economic Geology, Jackson School of Geosciences, Austin, Texas, USA. E-mail: tip.meckel@beg.utexas.edu.

[2]Formerly The University of Texas at Austin, Department of Geological Sciences, Jackson School of Geosciences, Austin, Texas, USA; presently Statoil, Houston, Texas, USA. E-mail: fmul@statoil.com.

Manuscript received by the Editor 19 June 2015; revised manuscript received 15 October 2015; published online 15 February 2016. This paper appears in *Interpretation*, Vol. 4, No. 1 (February 2016); p. SC35–SC49, 13 FIGS., 1 TABLE.

http://dx.doi.org/10.1190/INT-2015-0092.1.

(Holocene) depositional environments for use as reservoir analogs (similar to prior 2D studies; Posamentier and Kolla, 2003) is not widely published. Finally, HR3D systems have now been deployed (this study) in the context of subsurface geologic CO_2 storage assessment, focusing on potential fluid-migration pathways in the overburden above potential injection reservoirs.

The data and interpretations presented here focus on stratigraphic mapping (Quaternary evolution during a relative sea-level low- to highstand transition) and the associated extremely shallow (<100 m) gas anomalies (Mulcahy, 2015). Both of these topics are relevant for hydrocarbon prospect risking and drilling hazard assessment, although there is no active exploration in the study area at this time. The survey was collected in part to test a new technology (first P-Cable™ deployments in Gulf of Mexico [GoM]) and to study the near-offshore geology of the Texas Continental Shelf, in this case specifically for permanent storage of carbon dioxide (carbon capture and storage; Wallace et al., 2013). The objectives were to image the overburden above potential CO_2 storage reservoirs to determine seal continuity and the long-term fate of migrating fluids as related to deep-seated faults. These faults intersect the seafloor and the associated stratigraphy but are poorly imaged in conventional 3D data and are too deep for Chirp. However, the presentation here focuses on the technique, data quality, and ability to integrate shallow stratigraphic and fluid interpretations based on the HR3D data sets. As such, it serves as an example of similar application as may relate to the wide-ranging topics described above. Because these types of data sets are rare to date, the seismic interpretation community should benefit from the presentation of a well-studied example using this technology.

Figure 1. Regional satellite image with the 2013 HR3D survey shown in orange <10 miles offshore southern Galveston Island. Brazos River and Colorado River hydrologic zones are mapped in blue on the inset image. Images modified from Google Earth and Texas Water Development Board.

Geologic setting

The study area is on the inner shelf of the GoM just offshore San Luis Pass (SLP), Texas, at the western edge of the Galveston Bay and barrier island complex (Figure 1). The HR3D seismic survey location is slightly east of the Brazos River delta at Freeport, Texas, in water depths of 10–15 m. Based on the proximity of our study area to the modern Brazos River system, shallow stratigraphy in the study area is primarily associated with the paleo Brazos River system (Berryhill, 1986; Paine, 1991; Anderson et al., 1996; Abdullah et al., 2004). The Brazos River is a significant fluvial system that extends across Texas and spans multiple climate zones (Russell, 1945; Figure 1, inset). The Brazos River reaches the GoM at Freeport, Texas, with current typical discharge of approximately 10,000 cfs (approximately 280 m/s) with flood stage up to an order of magnitude greater. Similar contributions from multiple coastal rivers (e.g., Colorado, Brazos, Trinity) have resulted in the development throughout the Tertiary of an extensive, low-gradient, clastic-dominated shelf along the East Texas coast (Simms et al., 2007).

Quaternary geology

Simms et al. (2007) combine oxygen isotope data with radiometric sea-level datums (U/Th dates of corals) to create an accurate sea-level history for the GoM, ranging back 140 ka. The 140 ka period began with a relative glacial maximum, and a lowstand of 120 m below modern sea level (mbmsl; Lambeck and Chappell, 2001). This lowstand led to valley incision because the Brazos and Colorado River systems prograded out onto the exposed GoM shelf. From 135 to 120 ka, there was a rapid rise in sea level to approximately modern-day levels. Following this, there was a slow, oxygen isotope stage (OIS) 5 sea-level fall from 120 to 70 ka, resulting in delta lobe deposits across the GoM shelf. OIS 4 marks a relative minima of 80 mbmsl that lasted from 70 to 60 ka. The sea level continued to fall until approximately 20 ka, resulting in more delta lobe deposition on the shelf. At 20 ka, a second lowstand of 120 mbmsl occurred, producing the associated Brazos and Colorado incised valleys. The subsequent rapid rise in sea level led to present-day conditions (Simms et al., 2007).

Abdullah et al. (2004) specifically study the Late Quaternary Brazos delta system using high-resolution 2D seismic lines and sediment core and chronostratigraphic data. They map two unconformities, the deeper of which they

interpret as an incised valley associated with the OIS 6 lowstand (approximately 140 ka) and the shallower of which they relate to OIS 2 and the most recent lowstand (approximately 20 ka). Abdullah et al. (2004) are also able to map the location of the falling stage Brazos delta lobes that were deposited in the time between these periods of lowstand.

HR3D methods

Specific configurations of HR3D seismic technology have been developed over the past decade and are now becoming commercially available. The data were acquired using the P-Cable HR3D technology licensed and manufactured by Geometrics, Inc. This seismic system was developed by P-Cable 3D Seismic AS in Norway (S. Planke and F.N. Eriksen), with early deployments in cooperation with the National Oceanography Center (Southampton, UK), the University of Tromso, and GEOMAR (Petersen et al., 2010). One of the novel aspects of the newly developed HR3D systems is the ability to tow relatively short streamers (25–200 m) at close interstreamer spacing (6.25–12.5 m) without generating significant noise due to cross-cable strumming in the water. In particular, it is the very small bin sizes (e.g., <6.25 m^2), rather than the high-frequency content, that distinguish these type of data from a high-frequency data set with more conventional binning (e.g., 12.5–25 m^2). An early commercial version of the P-Cable system was deployed and operated by researchers of the Bureau of Economic Geology at the University of Texas at Austin, with logistical assistance from TDI-Brooks International and NCS Subsea (see the "Acknowledgments" section). The *R/V Brooks McCall*, operated primarily as a shallow sediment coring vessel supporting industry activities in the GoM, was mobilized in Freeport, Texas, to accommodate fit-to-purpose acoustic-source air compression, winch needs, and source-receiver geometry control (positioning) for this survey.

Table 1. HR3D seismic acquisition parameters.

Water depth	10–15 m
Streamers	12 × 25 m of solid core GeoEels
Channels	8 per streamer (96 total)
Streamer separation (inline)	12.5 m
Source	90 cubic inch GI air gun
Shot spacing	12.5 m
Bin size	6.25 × 6.25 m
Dominant frequency	150 Hz (50–250 typical range)

The acquisition geometry is defined by a "cross-cable" oriented perpendicular to the inline (transit) direction that connects twelve 25 m long streamers (Figure 2). A catenary shape for the cross cable is achieved using paravanes (diverters) at the ends of the cross cable. This acquisition geometry results in short-offset and low-fold data, one of the distinctions of this type of data. Source-receiver offsets are on the order of 100 m, and most common midpoint (CMP) gathers are populated by only 4–6 traces per bin (fold). Deployment and recovery operations were typically 2–3 h, and experience from three separate surveys (2012–2014) indicates acquisition efficiencies of approximately 60–100 line-km/day (4–7 km^2/day). Commercial production can surely improve on these operational metrics, but it is unlikely to be by more than a small factor. The 2013 SLP survey area is 31.5 km^2 (Figure 1). System specifications are listed in Table 1, and use solid-core GeoEel™ streamer technology.

Seismic resolution is defined by the ability of a data set to image features in the subsurface vertically and spatially. Vertically, seismic resolution is a function of source frequency content recorded by the receivers, with high-frequency returning energy providing higher resolution. The drawback of high-frequency data is the decrease in vertical penetration of the source energy, and therefore there is a decrease in the maximum imageable depth. For the survey described here, a single

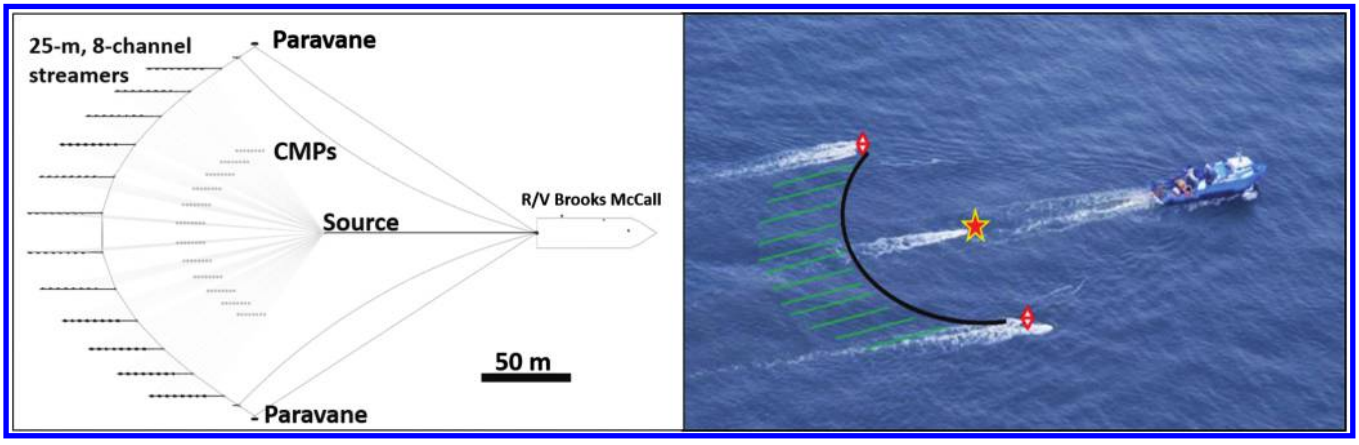

Figure 2. Left: Acquisition geometry and layback diagram (courtesy of NCS Subsea). Right: Interpreted aerial photo of the *R/V Brooks McCall* during acquisition in the GoM. Photo credit Eddie Tausch.

90 cubic inch generator-injector (GI) air gun source was used (peak frequency of 150 Hz), providing a high-quality image to depths of >500 ms TWT (approximately 380 m using a velocity of 1515 m/s). The zone of interest for this project is the shallowest 200 ms (approximately 150 m) corresponding to the past approximately 150 ky of sea-level change and associated erosion and deposition on the Texas shelf. Using a simple equation for vertical resolution (Ashcroft, 2011),

$$\text{Vertical resolution} = \frac{\left(\frac{1}{f} \times v\right)}{4}, \quad (1)$$

where $f = 150$ Hz (frequency) and $v = 1520$ m/s (velocity), we can calculate a vertical resolution of approximately 2.5 m for the 2013 HR3D data set. Older conventional commercial seismic surveys in the study area have a peak frequency of only 25 Hz, resulting in a vertical resolution of 15.2 m with the same sediment velocity (Figure 3).

For migrated data, the spatial resolution is predominantly controlled by the acquisition geometry. The shot interval and receiver spacing affect resolution in the inline direction, whereas streamer separation affects resolution in the crossline direction. The bin size for this survey was 6.25 m^2. Conventional 3D surveys typically have a bin size of 12 – 25 m^2, or approximately 4–16 times larger.

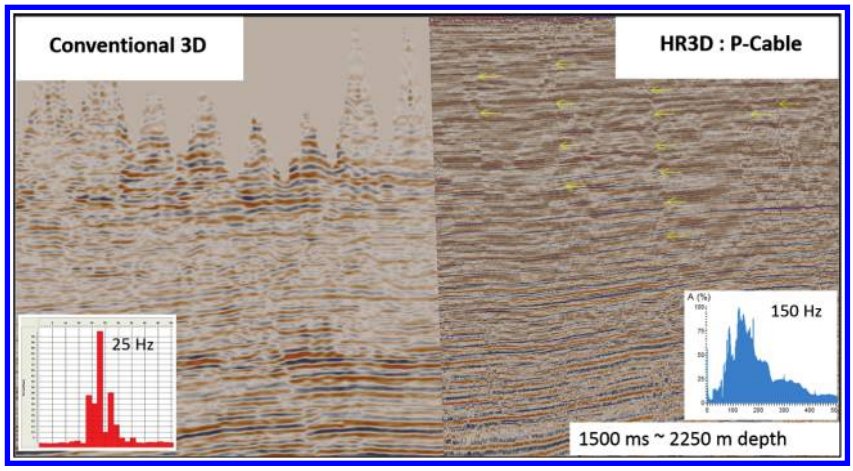

Figure 3. Comparison of conventional and HR3D vertical seismic resolution at an SLP site for a similar line. The inset plots show the frequency spectrum for the two data sets (taken from the central area of each image) and emphasize the high-frequency content of the HR3D data that provide for enhanced resolution. The high-frequency content of HR3D data may allow for vertical resolution <3 m, up to six times resolution improvement compared with conventional 3D in this case. Yellow arrows in HR3D data identify small-offset faults not visible in conventional data.

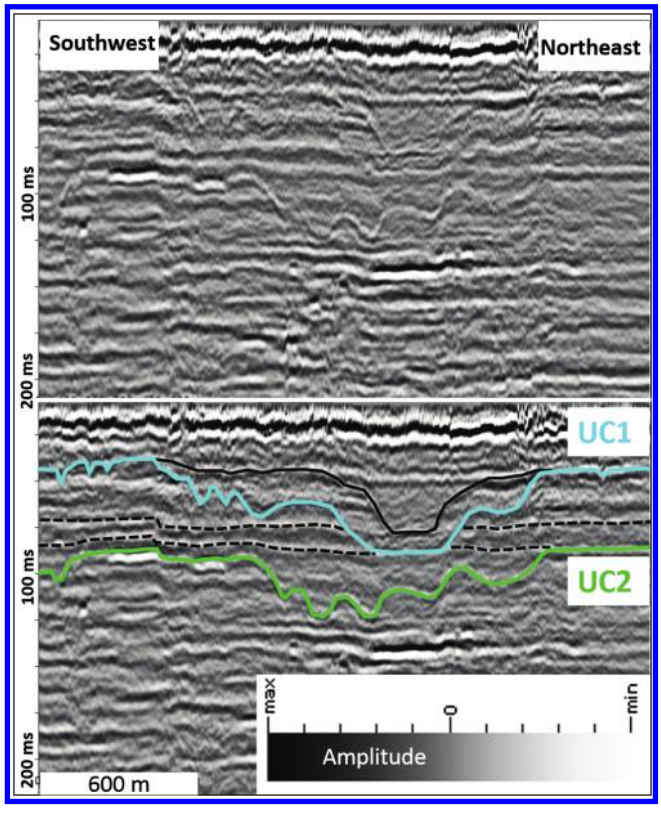

Figure 4. Example of an arbitrary inline (197; above) with interpretation (below). Interpreted surfaces UC1 and UC2 labeled. See the text for a description and interpretation.

Seismic mapping and interpretation

Seismic interpretation was performed using Halliburton's Decision Space Desktop and Schlumberger's Petrel. Seismic amplitude mapping was carried out by identifying key reflection characteristics such as truncation, onlap, and seismic facies (Catuneanu et al., 2009). Superposition and crosscutting relationships were used to interpret the relative timing of cutting and filling. The unconformities are identified as seismic events in which underlying strata have been truncated by overlying dipping reflections, often immediately overlain by chaotic/transparent facies.

Emphasis was put on mapping of the locally named UC1 and UC2 unconformities within the shallowest 150 ms (Figure 4). The shallowest erosional surface (UC1) is located at approximately 40 ms TWT (approximately 11 m below the seafloor, 1515 m/s), has a maximum relief of approximately 50 ms, and is associated primarily with a negative amplitude response. The deeper surface (UC2) is also primarily a negative amplitude located at approximately 90 ms TWT (approximately 50 m below the seafloor), with maximum relief of approximately 70 ms. These negative-amplitude responses have been modeled (Mulcahy, 2015) and may reflect an approximately 100 m/s decrease in seismic velocity to generate the negative response. The approximate depths for the UC1 and UC2 leave little doubt that the surfaces are correlative to those

mapped by Abdullah et al. (2004). The deeper UC2 unconformity is interpreted to be associated with the OIS 6 lowstand that occurred at approximately 140 ka, and the shallower UC1 unconformity is associated with OIS 2 and the most recent lowstand that occurred at approximately 20 ka. Figure 5 shows inlines 228 and 325 across the southwest–northeast extent of the 2013 survey (see Figure 1 for survey orientation and footprint), highlighting the mapped positions of UC1 and UC2.

Structural modification of the shallow interval of interest shows only subtle deformation because deposition was relatively recent. However, the mapping of subtle fault expression at shallow depths is a strength of HR3D methods (Crutchley et al., 2011; Brookshire et al., 2015). Structural features within our interval of interest include several steeply dipping normal faults and a shallow salt dome on the eastern side of the section. Four major normal faults are identified in the western portion of the study area focused on here, labeled N1 to N4 (left to right, Figure 5, top). Fault N1 trends northwest–southeast, is downthrown to the northeast, and has a maximum throw of approximately 6 m at the UC2 horizon. Fault N2 trends north–south, is downthrown to the east and has a maximum throw of approximately 4.5 m at UC2. Fault N3 trends northwest–southeast, is downthrown to the east, and has a maximum throw of approximately 4 m at UC2. Fault N3 trends north–south, is downthrown to the west, and has a maximum throw of approximately 3 m at UC2. Using an overlapping conventional 3D seismic survey that images below the P-Cable data, these faults are seen to originate at much deeper levels (up to 2.5 ms TWT) and are associated with a deep salt diapir feature and nonproductive antiformal, fault-bound reservoirs. However, these faults are unmappable with such precision in the conventional data for depths less than 500 ms, and in some cases they are unobserved altogether. The highly discontinuous and noisy section at the left-central side of the survey (Figure 5) and highlighted with red dashed lines is interpreted as a gas chimney system (discussed in a separate section).

Gridded maps of both shallow unconformities are shown corendered with the coherency attribute to

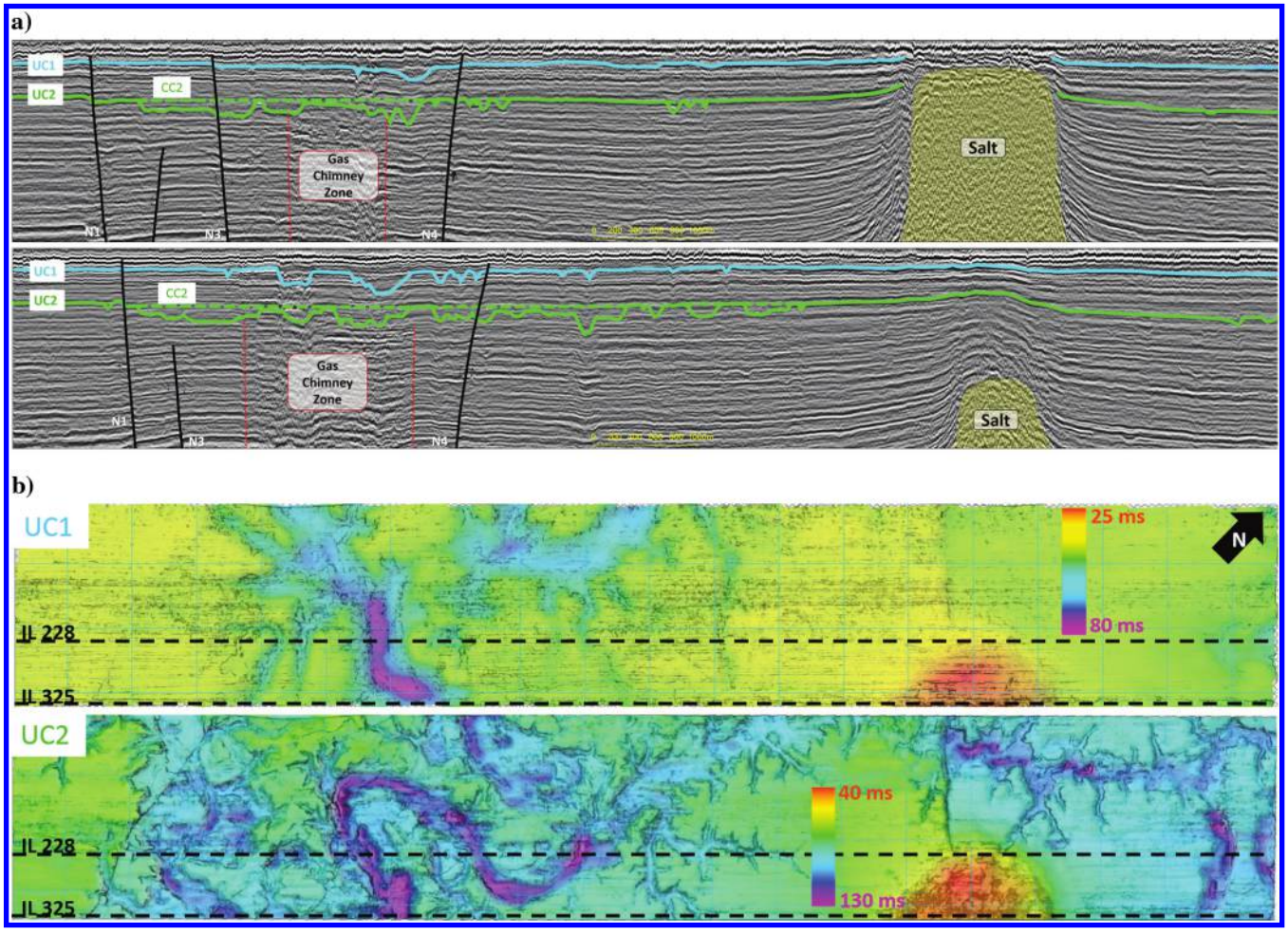

Figure 5. (a) Interpreted inlines 325 and 228 with fault and horizon interpretations. The vertical scale is 300 ms. The horizontal scale is 11 km. For the seismic amplitude scale, see Figure 4. (b) Surface maps for UC1 and UC2 corendered with semblance attribute to emphasize morphology definition.

highlight channel edges (Figure 5, bottom). The main channel of UC1 is oriented predominantly east–west, with several smaller and "straight" channels feeding into it. However, UC2 is characterized by a large north–south-flowing meandering channel (approximately 200 m max width) that connects with a smaller (approximately 100 m max width), west–east-meandering channel that is slightly off of the HR3D survey footprint, but it has been confirmed with an unpublished 2D high-resolution seismic line collected by the Institute for Geophysics at the University of Texas at Austin (S. Gulick, personal communication, 2015). Both channels have complex dendritic channel systems feeding into them, the most significant of which extends across the right side of the map to the northeast. The morphology and interpretation of UC2 and the interval directly above and below are discussed next.

Valley evolution

A horizon stratal slicing methodology was used for exploring valley evolution of the UC2 interval. The method involves slicing parallel to a single reference horizon with defined time shifts, and it assumes parallel seismic events (Zeng, 2007). This is an acceptable assumption for our interval because the structural deformation is limited and most reflections are parallel or only slightly subparallel. The reference horizon used is labeled CC2 in Figure 5 (the subhorizontal dashed green line slightly above UC2). This horizon was mapped by taking the correlative conformity of UC2 and connecting it across incisions, essentially creating an uppermost continuous "ceiling" for the channel forms. This process is equivalent to flattening the data volume on the CC2 horizon and looking at time slices within the flattened volume through the UC2 interval.

Figure 6 summarizes the valley evolution with two horizon maps and their interpretations. A meandering channel system is interpreted, with clearly identifiable point bars, channel scours, and lateral accretions, which expand into a wider, overlying estuarine system characterized by complex dendritic drainage features highlighted in the interpretations at the bottom of Figure 6. Interpretations of lithology and relative grain size are based on the seismic amplitude character in conjunction with the seismic horizon morphologies. For example, point bars and scours (channel lag deposits) within a meandering system can be interpreted as coarser gained deposits because of the way in which they form (Anderson and Anderson, 2010). Bernard et al. (1962) record silt, sand, and gravel sized grains at Brazos River point bar deposits on the late Quaternary Texas coastal plain. Point bars form as coarser-grained sediment is deposited in a zone of spatial deceleration along the inside of a channel bend. Channel lag deposits form after a channel segment has been scoured (typically at a meander bend), and coarse-grained sediment moves into and becomes trapped in the topographic lows associated with the deep scours (Anderson and Anderson, 2010). The seismically transparent character of the valley fill and the positive amplitude response at its top can be interpreted as any environment with a lack of impedance contrasts, but we prefer an interpretation of predominantly fine-grained, muddy fill. This transparent seismic character can be characteristic of transgressive open marine deposits (Reijenstein et al., 2011). This interpretation is also consistent with the context of the depositional analogs and seismic anomaly distribution (gas) presented below. A positive amplitude response is indicative of a positive change in impedance, and it would imply a higher velocity interval. This positive am-

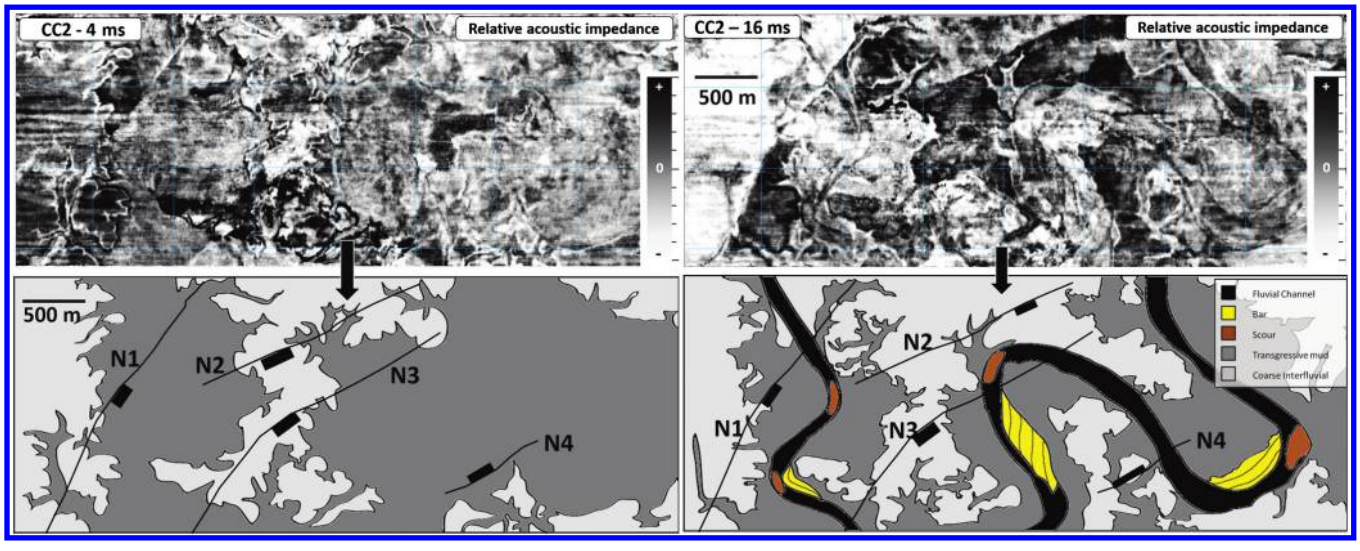

Figure 6. Relative acoustic impedance horizon slices at −16 ms and −4 ms below CC2 (see the top of Figure 5 for the surface location) representing the two major stages of valley evolution related to relative sea-level fluctuations (see the text for explanation). Interpretations are shown below each horizon slice, highlighting the transition from fluvial to estuarine environments.

plitude response can be characteristic of low-porosity mud-prone sediments (Maynard et al., 2010). The deposits of the previous sequence, capped by the negative amplitude response of the UC2 correlative conformity, are interpreted to be coarse grained based on the continuous and strong negative amplitude response (Suarez et al., 2008).

Figure 7 schematically summarizes a vertical 2D section sequence stratigraphic interpretation. The UC2 surface is associated with the OIS 6 lowstand (Abdullah et al., 2004). Eustatic sea level is estimated to have fallen more than 100 m during this time, exposing much of the GoM shelf (Simms et al., 2007). With the shelf exposed, river systems such as the Brazos prograded out onto the shelf, incising into shelfal deposits and forming incised valleys (Posamentier, 2001; Abdullah et al., 2004). Sediments deposited during this period of lowstand compose the lowstand systems tract (LST), and are commonly fluvial sands and coarse gravel (Allen and Posamentier, 1993; Catuneanu et al., 2009). In the case of the UC2 valley fill, LST deposits are minimal, such as in several channel scour deposits and some point bars. The minimal LST deposits can likely be explained by the upstream position of the UC2 system on the shelf because fluvial aggradation is generally much slower than in downstream sections (Allen and Posamentier, 1993). The rapid fall and rise of sea level during this period may not have allowed for significant fluvial aggradation (Simms et al., 2007). Transgressive systems tract (TST) and highstand systems tract (HST) deposits cannot be adequately distinguished using the SLP HR3D data set alone. Features that could aid in distinguishing the HST and TST such as estuarine point bars, tidal channels, tidal bars, and so on (Reijenstein et al., 2011) cannot be observed within the UC2 valley fill. As a result, the TST and HST are combined into a single unit for this interpretation. It is possible, with rapid transgression, that any estuarine processes were simply overwhelmed by the flooding of the system. The seismic facies that is observed within much of the UC2 valley fill is seismically transparent, likely indicative of muddy, open marine sediments, characteristic of the HST (Maynard et al., 2010; Reijenstein et al., 2011). Precise identification of the maximum flooding surface is difficult above the UC2 surface because there is a loss in data coherency moving vertically into the shallowest sections (<80 ms TWT). Above the HST deposits, Abdullah et al. (2004) describe deltaic deposits consistent with a falling stage systems tract (FST). Identifying these sequence stratigraphic surfaces and intervals allows for the prediction of facies types and comparisons to other studies looking at contemporaneous intervals throughout the Gulf Coast region (Bernard et al., 1970; Abdullah et al., 2004; Blum and Aslan, 2006; Simms et al., 2007). With these sequence stratigraphic predictions in mind, seismic facies analysis is used to corroborate the interpretations.

Seismic facies

Lithology and depositional environment interpretations made in the previous section rely on map-view amplitude contrasts that indicate changes in impedance. These interpretations can be corroborated by looking across the system in section view, in which several distinct seismic facies can be established. Seismic facies analysis interprets environmental setting and lithofacies based on the seismic reflection configuration (especially time-slice analysis), amplitude, continuity, frequency, and interval velocity (Mitchum et al., 1977). Four separate seismic facies were identified within the UC2 interval of interest and were characterized based on the reflection polarity, continuity, strength, and geometry. They include (1) coherent, subhorizontal, and strong amplitude response (negative at top) truncated by UC2 (coarse-grained interfluvial deposits of the previous sequence), (2) horizontal strong negative amplitude within the deepest sections of a meandering channel (coarse-grained channel scour deposits), (3) dipping/sigmoidal negative amplitude reflections on the inside of a meandering channel bend (coarse-grained fluvial point bar deposits), and (4) relative acoustic transparent intervals, often with positive response at the top, within a valley incision (transgressive estuarine/marine fine-grained mud fill). Several of these facies and their interpretations are illustrated in Figure 8. The channel system appears to be mostly mud filled with only several localized coarse-grained point bar and scour deposits.

Depositional analogs

Without the availability of shallow well log or core information at the SLP site, it is important to pursue

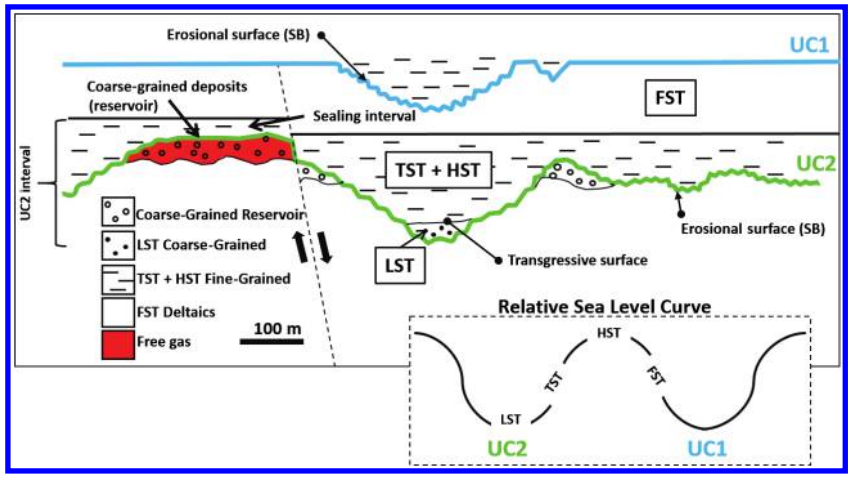

Figure 7. Conceptual model for the interpreted lithology and stratigraphic surfaces for the UC2 interval (labeled). Inset in lower right: schematic relative sea-level curve with timing of UC2 and UC1 sequence boundaries indicated.

other data sources to validate the seismic data interpretation presented here. This section will focus on outcrop analogs — taking what is well understood from similar, well-studied depositional systems and applying that information to the interpretations.

Understanding the scale and depositional/erosional processes of the UC2 system is the first step in identifying appropriate analogs. The UC2 system can be classified as a meandering channel type based on its plan-view morphology, with a maximum channel width of approximately 200 m, maximum channel depth of approximately 15–20 m, and a sinuosity (length of the channel for one wavelength/meander wavelength) of 2.85 (Ethridge and Schumm, 2007). Point bars with thicknesses up to approximately 12 m are observed, and maximum valley fill thickness is approximately 30 m.

Major lowstand fluvial systems with similar dimensions are exposed within the Upper Cretaceous Dunvegan Formation in Alberta, Canada (Plint and Wadsworth, 2003). The two largest channels observed within the Dunvegan have dimensions of 170×16 m (width × depth) and 150×28 m (Bhattacharya and MacEachern, 2009). Point bars within the sinuous channels of the Dunvegan measured up to 15 m and were typically >10 m. Figure 9 compares an aerial photograph of interpreted valley fill deposits from the Dunvegan Formation to a seismic section from the SLP HR3D with no vertical exaggeration through a meander bend. Not only does this image exemplify the ability of HR3D to identify such depositional structures at the outcrop scale as exemplified by the Dunvegan example, but it also highlights the similarities between the two systems. Both systems show horizontal basal deposits and laterally accreting features that are interpreted as point bars. In the case of the Dunvegan example, the basal deposits are coarse-grained, structureless sand, whereas the point bars are composed of sands and fine silts. This analog supports the interpretation of the UC2 scour deposits likely as more coarse grained and the point bar deposits as slightly finer grained.

A Holocene example of an incised valley that has been subsequently filled during transgression is the modern Gironde Estuary in southern France (Allen and Posamentier, 1993; Reijenstein et al., 2011). Similar to the Brazos River system, the Gironde Estuary resulted from the drowning of a fluvial system that formed during Holocene sea-level fall, and it has been well studied with abundant core and borehole data. The valley fill is composed of three separate depositional sequen-

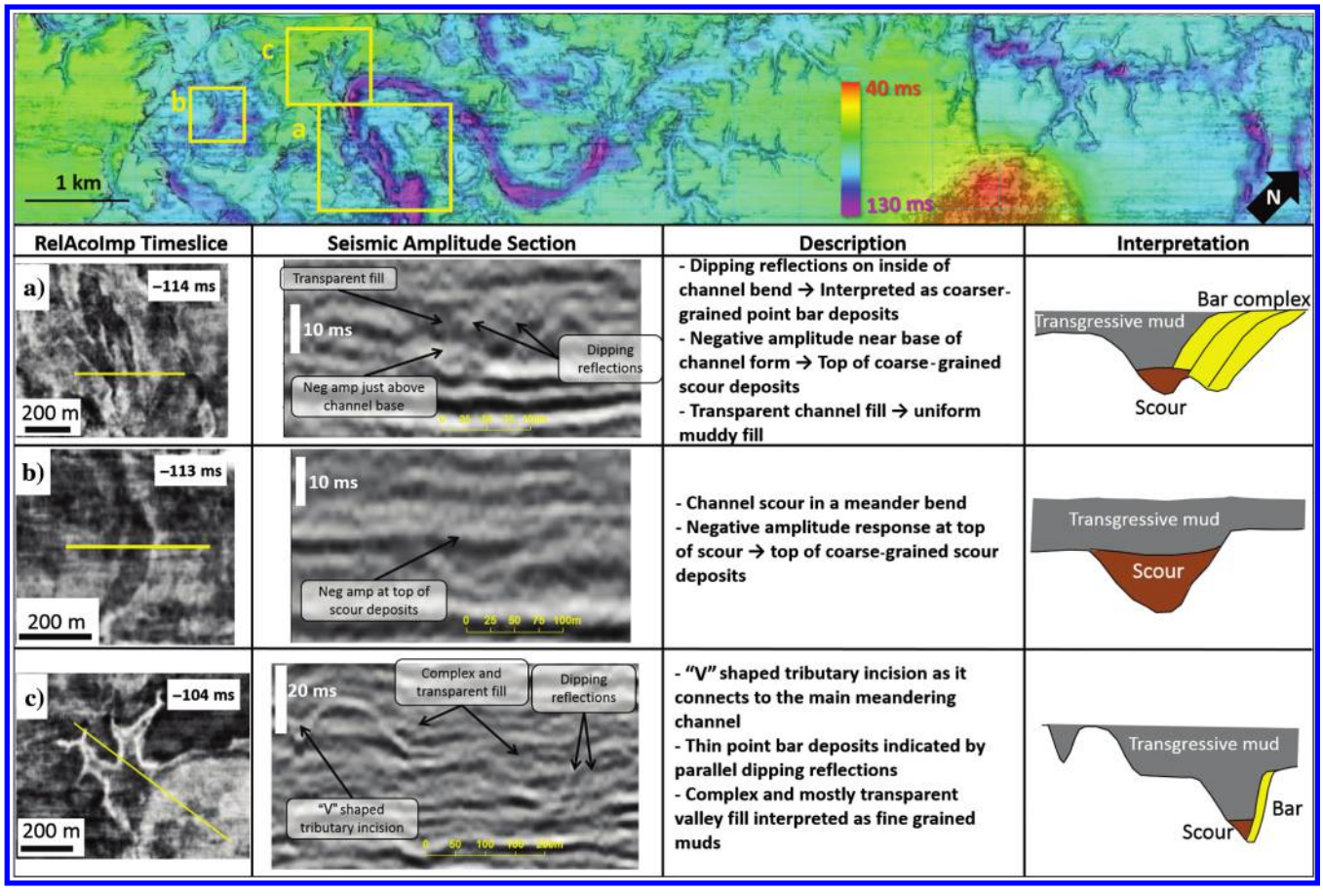

Figure 8. Channel characteristics and seismic facies for three different channel sections (a–c). The facies interpretations to the right are based on the seismic amplitude characteristics.

ces: one that accumulated during the last eustatic lowstand, one during the Holocene sea-level rise, and one during the present-day highstand. The thin lowstand deposits consist of fluvial sand and coarse sand directly in the channel thalweg. Transgressive and highstand deposits consist of tidal-estuarine sands and muds. The valley fill character of the Gironde Estuary is very similar to that observed at UC2 through seismic facies analysis — a thin, sandy interval present at only some locations within the channel thalweg, localized point bars, and a mostly fine grained transgressive fill.

Although the Dunvegan example represents a series of vertically stacked channels and mostly fluvial valley fill, indicative of a long-lived system, the UC2 and the Gironde valley fills show only a single channel-thick deposit (Allen and Posamentier, 1993). This single deposit could indicate a relatively short-lived fluvial system that functioned as a sediment bypass channel. In addition, the predominant transgressive mud fill indicates a rapid transgression in the UC2 case and at Gironde, in which the increase in accommodation overwhelmed the supply of fluvial sediment (Allen and Posamentier, 1993). Such an interpretation for UC2 is consistent with the glacial-eustatic sea-level curve (Simms et al., 2007), with a sea-level rise of 120 m over just 20,000 years. The rapid rise in sea level also adds to the preservation potential of the system (less time for erosional processes to occur) and most likely why so much of the UC2 system is preserved in the subsurface.

Seismic anomalies

Analysis of the shallowest intervals within active petroleum basins has become of increased interest over the past decade. Such interest largely stems from a pursuit to better understand hydrocarbon-migration processes and slope depositional models (Prather et al., 2012) and the increased availability of high-resolution seismic data (Foschi et al., 2014). A major interest in identifying shallow fluid anomalies, free gas and methane hydrates, is to reduce risks during hydrocarbon development operations (drilling and infrastructure development). Identifying shallow gas (seismically and through gas analyses of cores) can be used as an exploration tool for indicating the presence of deeper hydrocarbon prospects (Heggland, 1998), and we use anomaly identification at SLP to assist with understanding fluid systems in the context of future CO_2 sequestration projects. From a geotechnical perspective, shallow gas accumulations can reduce the shear strength in unlithified sediment and pose a significant drilling hazard (Andreassen and Odegaard, 2007). Shallow gas accumulations are also of interest in seismic processing and imaging because they can cause significant disruptions in data quality at the depth of the accumulation and generate a wipeout zone beneath it (Toth et al., 2014). Shallow gas migration through "pipes" or gas chimneys is also of increased interest because advancements in seismic acquisition and imaging technology have allowed for better observation and analysis of these features (Cartwright et al., 2007; Loseth et al., 2011).

Within seismic data, evidence for hydrocarbon accumulations is inferred based on the strongly negative amplitudes (bright spots). Fluid migration is interpreted based on the acoustic masking and discontinuous "pipes" within the seismic data (Andreassen and Odegaard, 2007). Loseth et al. (2009) summarize seismic amplitude characteristics of shallow accumulations and lay out a workflow for interpreting shallow amplitude anomalies related to hydrocarbon leakage. The workflow involves observation, description, and mapping of the anomalies before interpretation and identification of a leakage zone. This is the approach that is taken in the SLP HR3D study.

Within the shallowest approximately 250 ms of the SLP HR3D data set, multiple amplitude anomalies are present within a variety of stratigraphic settings. The anomalies are of high negative amplitude and reversed phase from the seafloor reflection. In several instances, phase shifts are observed along a continuous reflection, pushdown effects below the anomalies, and highly discontinuous, low-signal-to-noise areas directly below

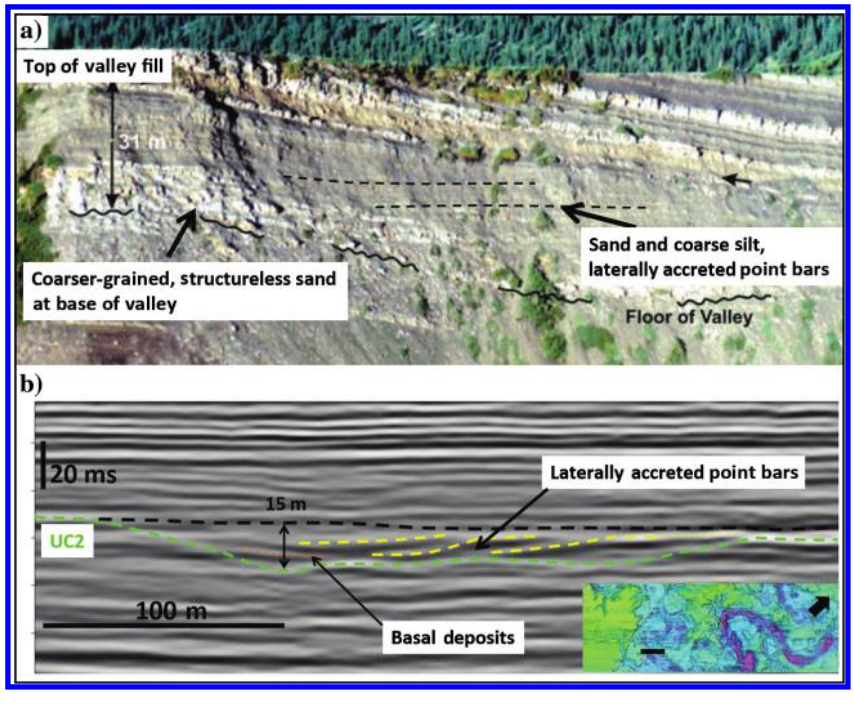

Figure 9. (a) Aerial photograph of an incised valley fill and lateral accretions, Dunvegan Formation, Alberta, Canada (from Plint and Wadsworth, 2003). (b) Inline 243 from SLP HR3D (minimized vertical exaggeration) highlighting interpreted valley fill and lateral accretions similar to the Canadian example.

the anomalies. Based on these observations, these high-amplitude anomalies are interpreted as "bright spots" indicative of free phase gas (likely methane) accumulations. Given the association with a vertical seismic anomaly that can be linked to a deeper antiform using convention 3D seismic data, the gas in interpreted to be of thermogenic origin (deep hydrocarbon source; see below).

The amplitude anomalies identified within the SLP HR3D data set exhibit strong negative amplitude responses, indicative of a large decrease in sediment velocity. Such large negative-amplitude responses are consistent with the hypothesis that these anomalies are the result of gas accumulations; however, on its own, it is not a confirmation of the hypothesis. Figure 10 shows the seismic expression of several of these amplitude anomalies in a 2D section. Figure 10a presents a single, strong negative-amplitude anomaly at approximately 92 ms, and the response is coherent laterally until it is truncated on either edge by the UC2 unconformity. Figure 10b highlights multiple amplitude anomalies ranging from approximately 90 to 150 ms. Multiple positive to negative phase shifts are observed in this example, with stacking of anomalies and a highly discontinuous zone below the 142 ms anomaly that could be indicative of fluid migration. Finally, in Figure 10c, a laterally extensive anomaly is observed that is truncated by erosional features belonging to the UC2 unconformity. Within the UC2 interval, these anomalies appear confined by the UC2 unconformity; that is, the anomalies exist in areas that have not been eroded. For the deeper, 142 ms anomaly (Figure 10b), however, the amplitudes are less confined, as indicated by the vertical stacking and larger lateral extent.

Observations from these examples include strong negative amplitudes, phase shifts, stacked anomalies, frequency reduction, and pushdown below some of the anomalies; all of these features can be indicative of gas accumulation (Andreassen and Odegaard, 2007; Loseth et al., 2009; Foschi et al., 2014). Furthermore, the discontinuous zone noted in Figure 10b is characterized by chaotic reflections and could be indicative of past fluid migration (Cartwright et al., 2007; Loseth et al., 2011).

Although identifiable in a 2D section, the amplitude anomalies are most apparent in horizontal time slices (Figure 11). Seismic amplitude, root mean square (rms) amplitude, and sweetness were all valuable in determining the extent and characteristics of the shallow anomalies (Chopra and Marfurt, 2007). The rms amplitude is defined as the square root of the average over a defined vertical time window (9 ms in this case) of the squared values of the waveform, and it can be used to identify channels (Janocko et al., 2013). Sweetness is derived by combining instantaneous frequency and reflection strength (Hart, 2008). In Figure 11, we note the ability of rms and sweetness attributes to significantly increase the ability to visualize the amplitude anomalies and their extent. Better visualization is the result of the rms and sweetness algorithms providing absolute value amplitude information and calculating over a vertical window, rather than for a specific TWT. Also, the rms amplitude will provide a better sense of the total lateral extent of each anomaly, whereas an individual time slice might only show a portion of its extent.

These seismic attributes aforementioned can also be used to extract 3D shapes (often referred to as "geobodies" in seismic interpretation) of the anomalies to better understand their distribution and characteristics. A geobody is an interpreted 3D shape enveloping similar seismic amplitudes (or other attributes). For the HR3D data, extracted geobodies represent a contiguous similar rms amplitude response in 3D. Geologically, they are interpreted to represent similar rock properties

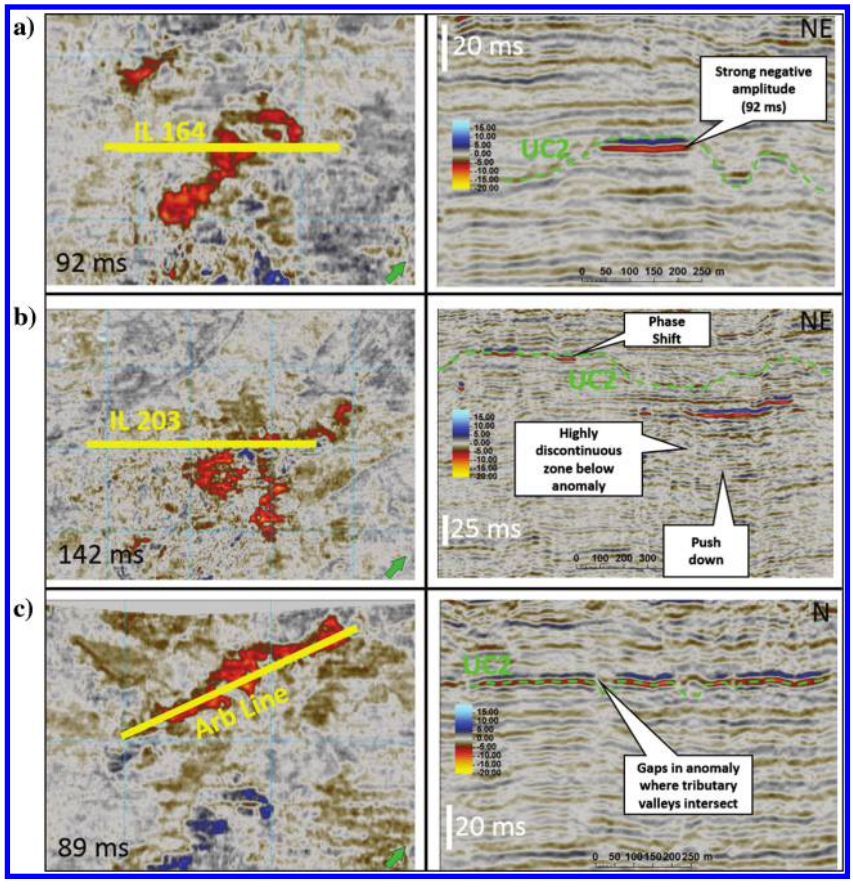

Figure 10. (a-c) Various examples of maps and 2D sections highlighting the seismic expression of amplitude anomalies.

(e.g., facies, gas charge, and salt). Geobodies were extracted by selecting a subvolume within the seismic volume that included all of the amplitude anomalies (excluding the water-bottom reflection, which is a quite-large amplitude itself) and then isolating voxels (3D data points) that have rms values above a specified threshold (Figure 12 outlines the extraction process). The rms amplitude threshold value used was 4 because this value generated coherent geobodies for all depth intervals of interest. As can be seen in the histogram, rms values greater than 4 are at the very high end of the distribution (uppermost 0.3% of values). Geobodies are colored by elevation (Figure 12), and they range in TWT (depth) from 170 ms (approximately 110 m) to 40 ms (approximately 11.5 m). The geologic significance of these geobody representations of the seismic anomalies is interpreted below.

Anomaly interpretation within stratigraphic context

The rms amplitude anomalies (geobodies) exist within several different stratigraphic settings. They range in maximum horizontal length from 1000 to less than 30 m. Because all of the anomalies are less than half a seismic cycle thick vertically, it is impossible to establish their exact thicknesses in meters. However, their maximum thickness is likely less than 3 m because a separate basal response is generally not observed, consistent with the known frequency and velocity constraints (vertical resolution; see the "HR3D methods" section). The largest and deepest (900 m across) anomaly sits within what is interpreted to be a set of sandy beach ridges, based on the plan-view morphological interpretation (Figure 11 at 144 ms; top). A very small (<30 m width) meandering channel appears as

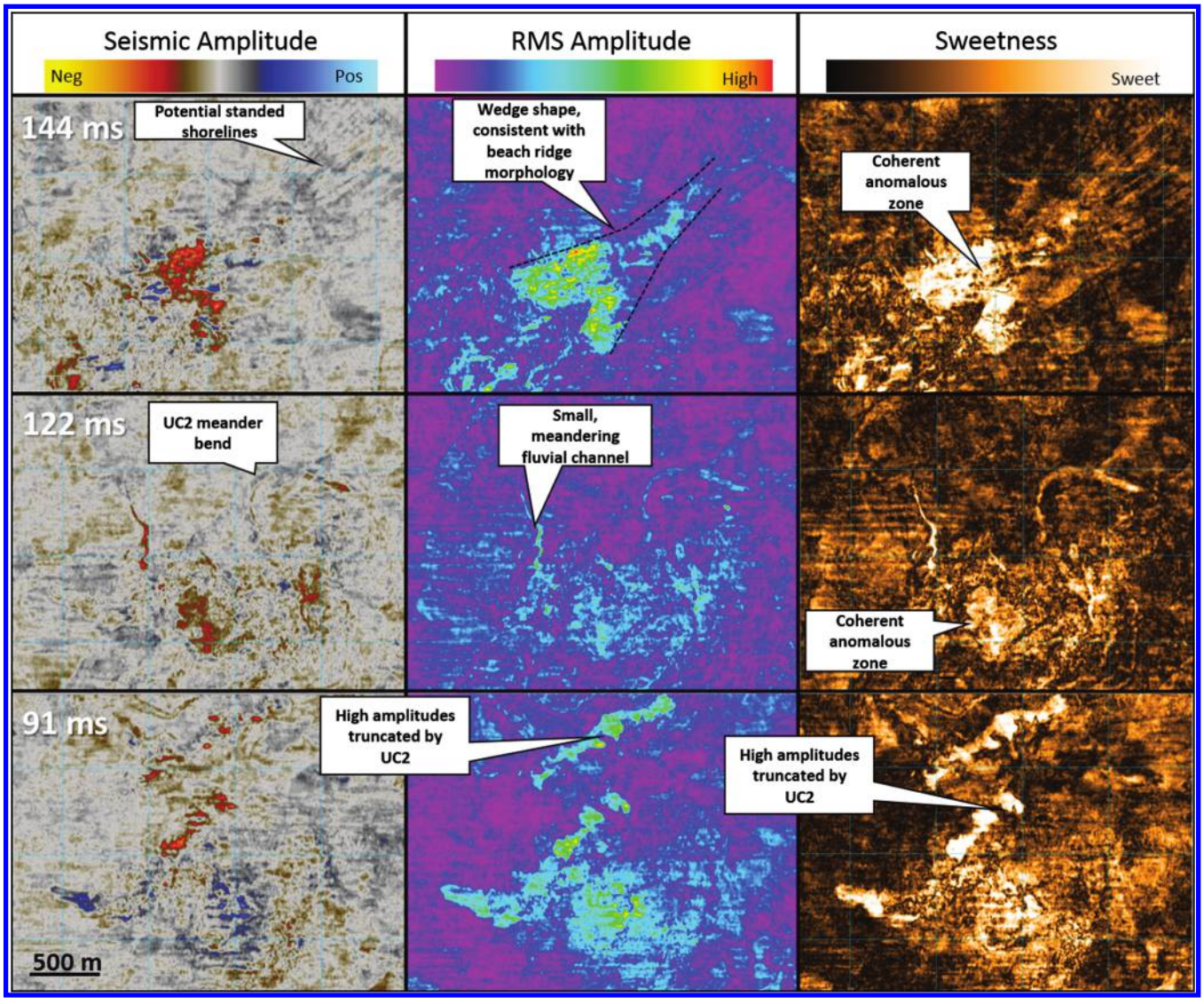

Figure 11. Amplitude anomalies imaged at various TWT (144, 122, and 91 ms, top to bottom) with rms and sweetness attributes for comparison to the right. See the text for attribute definitions.

a seismically bright spot at approximately 122 ms and connects to another, slightly shallower anomaly. Gas likely migrated through this porous channel to fill an updip reservoir, although a full analysis of fluid-migration pathways remains to be performed. The next large set of anomalies sits directly within the UC2 interval; they range in maximum length from 400 to 1000 m. However, these anomalies do not exist within the "sandy" channel features interpreted in the thalweg (scours, point bars, etc.), but rather within the interfluvial zones beyond the channel margins. Although unexpected based on the classic fluvial reservoir models, this fits with our stratigraphic interpretation of the interval — a predominantly mud-filled incised valley, with coarse-grained interfluvial deposits from a previous sequence existing laterally. The interfluvial deposits function as a reservoir that has been eroded by valley incision to produce several discrete remnant topographic highs. The fine-grained transgressive fluvial valley fill acts as a sealing interval above the interfluvial reservoir.

Many of these interpretations are enhanced by overlying the amplitude geobodies on a variance attribute time slice (Figure 13a). Note that most of the anomalies are located directly above or adjacent to the vertical gas chimney zone (dashed outline). The anomaly locations directly support the hypothesis that the seismically discontinuous zone is a deep thermogenic gas chimney that has sourced these shallow gas accumulations. Thermogenic gas migration to a shallow depth is supported by gas analyses of recent shallow sediment cores at the site that have carbon isotope composition ($\delta^{13}C$ of $CH_4 > -50$) consistent with thermogenic gas, but with some biodegradation. In addition, cases are observed in which anomalies align along steeply dipping normal faults that appear to provide a fault seal and footwall structure to several of the accumulations. When the UC2 structure map is overlain (Figure 13b), the shallow accumulations are restricted to remnant topographic highs that have been established due to erosion (note how the accumulation conforms around the tributary valleys) and normal faulting (accumulations are on the footwall of normal faults).

The presence of a gas chimney and shallow gas accumulations has implications for the permanent storage of carbon dioxide, which has been considered for the area (Wallace et al., 2013). One of the applications of HR3D is to investigate the overburden above potential CO_2 storage sites to characterize potential fluid-migration pathways. Given the obviously established fluid-migration pathway from depth identified in the SLP HR3D

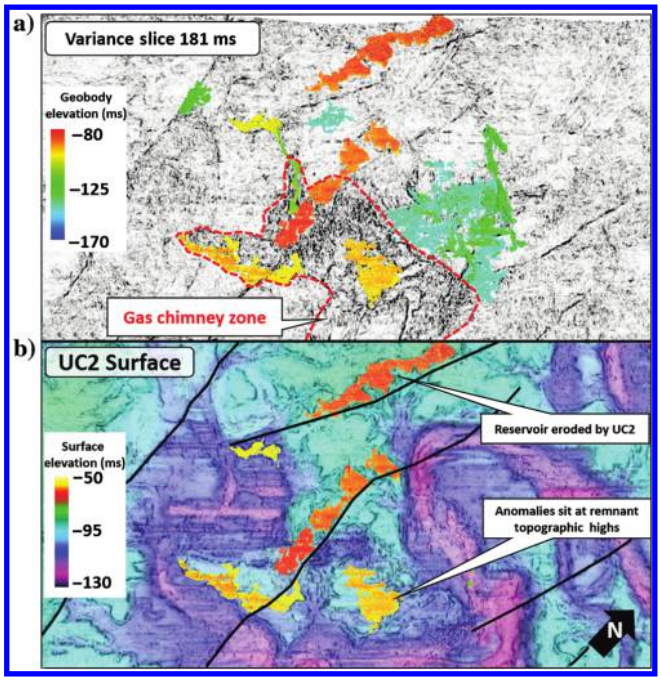

Figure 13. Map view of rms amplitude geobodies. (a) Geobodies colored by elevation (ms) overlain on a horizontal variance time slice at 181 ms. (b) Geobodies overlain on a UC2 time structure map (colored with scale shown, different than anomalies). Note the location of anomalies along faults and within the remnant topographic highs of the pre-UC2 stratigraphic interval.

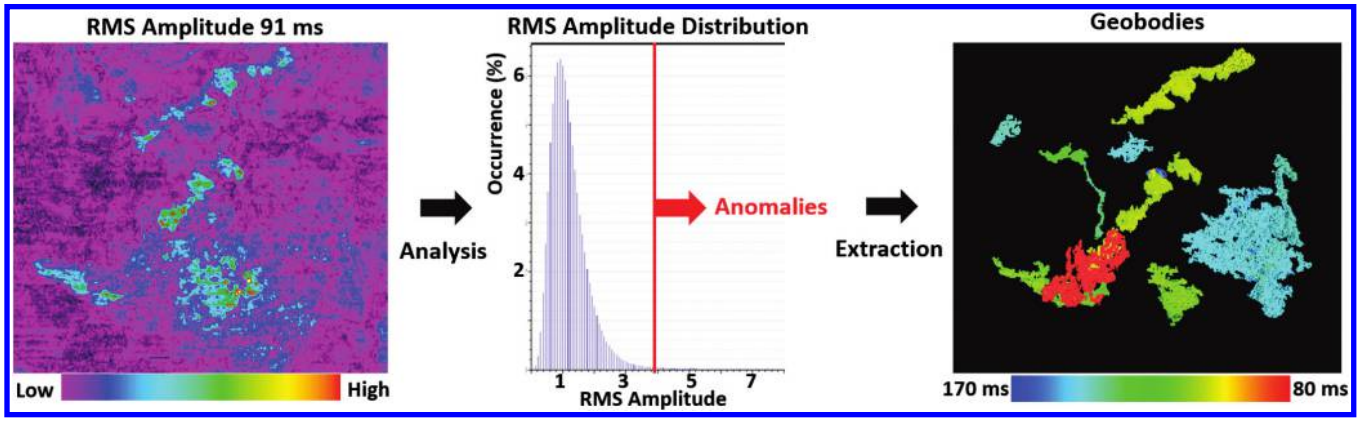

Figure 12. Extraction process to isolate anomalous amplitude events. Histogram (center) shows rms amplitude distribution and cutoff (4, representing uppermost 0.3% of values) for similar rms amplitude (geobody) extraction. Geobodies in the right image are colored according to elevation (TWT) between 170 (blue) and 80 ms (red).

survey, the site has been removed from a list of potential candidate sites.

Conclusions

The first deployment of the P-Cable HR3D seismic acquisition system in the GoM images the upper 500 ms in unprecedented resolution, allowing for detailed visualization and interpretation of Quaternary stratigraphy associated with relative sea level change. The mapped UC1 and UC2 unconformities are interpreted to be incised valley associated with the OIS 2 and OIS 6 lowstands, respectively. Sediment fill within the UC2 valley is interpreted to consist of predominantly TST/HST finer-grained deposits, with several more coarse-grained point bar and channel scour deposits associated with the LST. Amplitude anomalies exist within the shallowest 200 ms of the data volume and are interpreted as thermogenic free gas accumulations that have migrated from depth. Free gas charges extremely shallow lithologies such as interfluves associated with the UC1 and UC2 incised valleys, a small fluvial channel, and two stranded shorelines (beach ridges). Structural, stratigraphic, and combination traps are observed, although none are economic. However, a more detailed understanding of shallow stratigraphy and structure and fluid systems is important for understanding basin fluid systems and geotechnical drilling hazards. The identification of gas-migration features is considered important for characterizing permanent subsurface storage settings for CO_2 storage. In the case of this example, the deeper stratigraphy below the gas chimney and shallow reaccumulations was removed from further consideration for CO_2 injection.

Acknowledgments

This material is based on research supported by the Department of Energy National Energy Technology Laboratory under award number DE-FE0001941. Financial support for the research was also provided by the Texas General Land Office. Excellent project management was provided by K. Kluger (DOE) and R. Treviño (BEG). We acknowledge the use of the P-Cable technology (Norwegian patent no. 317652) manufactured by Geometrics. B. Hoff played an instrumental role in connecting UT-Austin researchers and vessel operator TDI-Brooks International. The HR3D seismic acquisition was undertaken in collaboration with TDI-Brooks International, NCS Subsea, GeoSurvey Systems, and Alpha Seismic Compression. In particular, we wish to thank D. Brooks and the crew of the *R/V Brooks McCall* for vessel support. Seismic acquisition and processing were assisted by Nathan Bangs and Tom Hess (UTIG) and Finn Michelsen (GeoSurvey Systems). Additional processing was undertaken by W. Adams at Reservoir Definition, Inc. B. Brookshire led navigation/positioning for NCS Subsea. Paravane consultation was provided by G. Barker and array modeling by D. Martin of Global Dynamics, Inc. Deployment and acquisition assistance during three surveys between 2012 and 2014 was provided by L. Moscardelli (now at Statoil) and D. Dunlap from the bureau of economic geology, and graduate students from the University of Texas at Austin-Jackson School of Geosciences (D. Eakin, M. Duncan, S. Porse, and J. Osmond) and Southern Methodist University (B. Phrampus).

References

Abdullah, K., J. Anderson, J. Snow, and L. Holdford-Jack, 2004, The Late Quaternary Brazos and Colorado Deltas, Offshore Texas, USA — Their evolution and the factors that controlled their deposition: SEPM Special Publication 79, 237–269.

Allen, G., and H. Posamentier, 1993, Sequence stratigraphy and facies model of an incised valley fill: The Gironde Estuary, France: Journal of Sedimentary Petrology, **63**, 378–391.

Anderson, J. B., K. Abdullah, S. Sarzalejo, F. Siringan, and M. A. Thomas, 1996, Late Quaternary sedimentation and high-resolution sequence stratigraphy of the east Texas shelf, *in* M. de Batist, and P. Jacobs, eds., Geology of siliciclastic seas: Geological Society of London, Special Publication, **117**, 95–124.

Anderson, R., and S. P. Anderson, 2010, Geomorphology: The mechanics and chemistry of landscapes, 1st ed.: Cambridge University Press.

Andreassen, K., and C. Odegaard, 2007, Analysis of shallow gas and fluid migration within the Plio-Pleistocene sedimentary succession of the SW Barents Sea continental margin using 3D seismic data: Geo-Marine Letters, **27**, 155–171, doi: 10.1007/s00367-007-0071-5.

Ashcroft, W., 2011, A petroleum geologist's guide to seismic reflection, 1st ed.: Wiley-Blackwell.

Bernard, H., R. LeBlanc, and C. Major, 1962, Recent and Pleistocene geology of southeast Texas, field excursion no. 3, *in* Geology of the Gulf Coast and central Texas, and guidebook of excursions: Houston Geological Society, 175–224.

Bernard, H., C. F. Major, Jr., B. S. Parrott, and R. J. Le Blanc Sr., 1970, Recent sediments of southeast Texas: A field guide to the Brazos alluvial and deltaic plains and the Galveston barrier island complex: Guidebook Number 11: Bureau of Economic Geology.

Berryhill, H. L., Jr., 1986, Later Quaternary facies and structure, northern Gulf of Mexico: Interpretations from seismic data: AAPG Studies in Geology 23.

Bhattacharya, J., and J. MacEachern, 2009, Hyperpycnal rivers and prodeltaic shelves in the Cretaceous seaway of north America: Journal of Sedimentary Research, **79**, 184–209, doi: 110.2110/jsr.2009.026.

Blum, M., and A. Aslan, 2006, Signatures of climate vs. sea-level change within incised valley-fill successions: Quaternary examples from the Texas Gulf Coast: Sedimentary Geology, **190**, 177–211, doi: 10.1016/j.sedgeo.2006.05.024.

Brookshire, B. N., Jr., F. P. Landers, and J. A. Stein, 2015, Applicability of ultra-high-resolution 3D seismic data

for geohazard identification at mid-slope depths in the Gulf of Mexico — Initial results: Underwater Technology, **32**, 271–278, doi: 10.3723/ut.32.271.

Cartwright, J., M. Huuse, and A. Aplin, 2007, Seal bypass systems: AAPG Bulletin, **91**, 1141–1166, doi: 10.1306/04090705181.

Catuneanu, O., V. Abreu, J. P. Bhattacharya, M. D. Blum, and R. W. Dalyrymple, 2009, Towards the standardization of sequence stratigraphy: Papers in the Earth and Atmospheric Sciences, Issue Paper 238, 1–33.

Chopra, S., and K. J. Marfurt, 2007, Seismic attributes for prospect identification and reservoir characterization: SEG Geophysical Developments Series No. 11.

Crutchley, G. J., C. Berndt, D. Klaeschen, and D. G. Masson, 2011, Insights into active deformation in the Gulf of Cadiz from new 3D seismic and high-resolution bathymetry data: Geochemistry, Geophysics, Geosystems, **12**, 1–20, doi: 10.1029/2011GC003576.

Ebuna, D. R., T. J. Mitchell, P. J. Hogan, S. Nishenko, and H. G. Greene, 2013, High-resolution offshore 3D seismic geophysical studies of infrastructure geohazards: 26th Symposium on the Application of Geophysics to Engineering and Environmental Problems, SAGEEP 2013, Environmental and Engineering Geophysical Society, 311–320.

Ethridge, F., and S. Schumm, 2007, Fluvial seismic geomorphology: A view from the surface: Geological Society, London, Special Publications, **277**, 205–222, doi: 10.1144/GSL.SP.2007.277.01.12.

Foschi, M., J. A. Cartwright, and F. J. Peel, 2014, Vertical anomaly clusters: Evidence for vertical gas migration across multilayered sealing sequences: AAPG Bulletin, **98**, 1859–1884, doi: 10.1306/04051413121.

Gutowski, M., J. M. Bull, J. K. Dix, T. J. Henstock, P. Hogarth, T. Hiller, T. G. Leighton, and P. R. White, 2008, Three-dimensional high-resolution acoustic imaging of sub-seabed: Applied Acoustics, **69**, 412–421, doi: 10.1016/j.apacoust.2006.08.013.

Hart, B. S., 2008, Channel detection in 3-D seismic data using sweetness: AAPG Bulletin, **92**, 733–742, doi: 10.1306/02050807127.

Heggland, R., 1998, Gas seepage as an indicator of deeper prospective reservoirs — A study based on exploration 3D seismic data: Marine and Petroleum Geology, **15**, 1–9, doi: 10.1016/S0264-8172(97)00060-3.

Janocko, M., W. Nemec, S. Henriksen, and M. Warchol, 2013, The diversity of deep-water sinuous channel belts and slope valley-fill complexes: Marine and Petroleum Geology, **41**, 7–34, doi: 10.1016/j.marpetgeo.2012.06.012.

Lambeck, K., and J. Chappell, 2001, Sea level change through the last glacial cycle: Science, **292**, 679–686, doi: 10.1126/science.1059549.

Loseth, H., M. Gading, and L. Wensaas, 2009, Hydrocarbon leakage interpreted on seismic data: Marine and Petroleum Geology, **26**, 1304–1319, doi: 10.1016/j.marpetgeo.2008.09.008.

Loseth, H., L. Wensaas, B. Arntsen, N.-M. Hanken, C. Basire, and K. Grau, 2011, 1000 m long gas blow-out pipes: Marine and Petroleum Geology, **28**, 1047–1060, doi: 10.1016/j.marpetgeo.2010.10.001.

Marsset, B., T. Missiaen, Y.-H. De Roeck, M. Noble, W. Versteeg, and J. P. Henriet, 1998, Very high resolution 3D marine seismic data processing for geotechnical applications: Geophysical Prospecting, **46**, 105–120, doi: 10.1046/j.1365-2478.1998.00076.x.

Maynard, J., H. Feldman, and R. Alway, 2010, From bars to valleys: The sedimentology and seismic geomorphology of fluvial to estuarine incised-valley fills of the grand rapids formation (lower cretaceous), Iron River Field, Alberta Canada: Journal of Sedimentary Research, **80**, 611–638, doi: 10.2110/jsr.2010.060.

Mitchum, R., P. Vail, and J. Sangree, 1977, Seismic stratigraphy and global changes of sea level, part 6: Stratigraphic interpretation of seismic reflection patterns in depositional sequences, *in* C. E. Payton, ed., Seismic stratigraphy — Applications to hydrocarbon exploration: AAPG Memoir 26, 117–133.

Mulcahy, F. J., 2015, Use of high-resolution 3D seismic data to evaluate Quaternary valley evolution during transgression, Offshore San Luis Pass, Gulf of Mexico: M. S. thesis, The University of Texas at Austin.

Paine, J. G., 1991, Late Quaternary depositional units, sea level, and vertical movement along the central Texas coast: Ph.D. thesis, The University of Texas at Austin.

Petersen, C. J., S. Buenz, S. Hustoft, J. Mienert, and D. Klaeschen, 2010, High-resolution P-Cable 3D seismic imaging of gas chimney structures in gas hydrated sediments of an Arctic sediment drift: Marine and Petroleum Geology, **27**, 1981–1994, doi: 10.1016/j.marpetgeo.2010.06.006.

Pirmez, C., B. E. Prather, G. Mallarino, W. W. O'HAyer, A. W. Droxler, and C. D. Winker, 2012, Chronostratigraphy of the Brazos-Trinity depositional system, western Gulf of Mexico: Implications for deepwater depositional models, *in* B. E. Prather, M. E. Deptuck, D. Mohrig, B. Van Hoorn, and R. B. Wynn, eds., Application of the principles of seismic geomorphology to continental-slope and base-of-slope systems: Case studies from seafloor and near-seafloor analogues: SEPM Special Publication 99, 111–143.

Plint, A., and J. Wadsworth, 2003, Sedimentology and paleogeomorphology of four large valley systems incising delta plains, western Canada Foreland Basin: Implications for mid-Cretaceous sea-level changes: Sedimentology, **50**, 1147–1186.

Posamentier, H. W., 2001, Lowstand alluvial bypass systems: Incised vs. unincised: AAPG Bulletin, **85**, 1771–1793.

Posamentier, H. W., and V. Kolla, 2003, Seismic geomorphology and stratigraphy of depositional elements in deep-water settings: Journal of Sedimentary Research, **73**, 367–388, doi: 10.1306/111302730367.

Prather, B. E., M. E. Deptuck, D. Mohrig, B. Van Horn, and R. B. Wynn, 2012, Application of the principles of seismic geomorphology to continental-slope and base-of-slope systems: Case studies from seafloor and near-seafloor analogues: SEPM Special Publication 99, 383.

Reijenstein, H., H. Posamentier, and J. Bhattacharya, 2011, Seismic geomorphology and high-resolution seismic stratigraphy of inner-shelf fluvial, estuarine, deltaic, and marine sequences, Gulf of Thailand: AAPG Bulletin, **95**, 1959–1990, doi: 10.1306/03151110134.

Russell, R., 1945, Climates of Texas: Annals of the Association of American Geographers, **35**, 37–52, doi: 10.1080/00045604509357268.

Simms, A., K. Anderson, Z. Taha, and J. Wellner, 2007, Geomorphology and the age of the oxygen isotope stage 2 (last lowstand) sequence boundary on the northwestern Gulf of Mexico continental shelf: Geological Society of London, 29–46.

Suarez, Y., K. J. Marfurt, and M. Falk, 2008, Seismic attribute-assisted interpretation of channel geometries and infill lithology: A case study of Anadarko Basin Red Fork channels: 78th Annual International Meeting, SEG, Expanded Abstracts, 963–967.

Toth, Z., V. Speib, and J. Jensen, 2014, Seismo-acoustic signatures of shallow free gas in the Bornholm Basin, Baltic Sea: Continental Shelf Research, **88**, 228–239, doi: 10.1016/j.csr.2014.08.007.

Wallace, K. J., T. A. Meckel, D. L. Carr, R. H. Trevino, and C. Yang, 2013, Regional CO_2 sequestration capacity assessment for the coastal and offshore Texas Miocene interval: Greenhouse Gases: Science and Technology, **4**, 53–65, doi: 10.1002/ghg.1380.

Zeng, H., 2007, Seismic imaging for seismic geomorphology beyond the seabed: Potentials and challenges, *in* R. J. Davies, H. W. Posamentier, L. J. Wood, and J. A. Cartwright, eds., Seismic geomorphology: Applications to hydrocarbon exploration and production: Geolgical Society, London, Special Publications 277, 15–28.

Tip Meckel received an M.S. (1998) in geology from the University of Montana in Missoula and a doctorate (2003) in geology and geophysics from the University of Texas at Austin. He subsequently taught undergraduate geology at Colby College in Maine followed by a two-year position with the U.S. Geological Survey as a Mendenhall postdoctoral fellowship in Woods Hole, Massachusetts, USA. Since 2006, he has been a research scientist investigating geologic carbon sequestration topics for the Bureau of Economic Geology at the University of Texas at Austin.

Francis Mulcahy received a B.S. (2010) in science of earth systems from Cornell University and an M.S. (2015) in geology from the Jackson School of Geosciences at the University of Texas at Austin. He is currently working as an exploration geologist at Statoil in Houston, Texas, USA. He spent several years working as a processing geophysicist at WesternGeco in between degrees.